Millennial variability of terrigenous transport to the central-southern Peruvian margin during the last deglaciation (18-13 kyr BP)

Marco Yseki[1], Bruno Turcq[1], Sandrine Caquineau[1], Renato Salvatteci[2], José Solis[3], C. Gregory Skilbeck[4], Federico Velazco[5] and Dimitri Gutiérrez[3,5]

[1]IRD, LOCEAN-IPSL, Laboratoire d'Océanographie et du Climat: Expérimentation et Approches Numériques, Sorbonne Université, CNRS, IRD, MNHN, Paris, France.
[2]Center for Ocean and Society, Kiel University, Kiel, 24105, Germany.
[3]Laboratorio de Ciencias del Mar, Facultad de Ciencias y Filosofía, Universidad Peruana Cayetano Heredia, Lima, Peru.
[4]Faculty of Science, University of Technology Sydney. PO Box 123 Broadway, Sydney NSW. 2007.
[5]Dirección General de Investigaciones Oceanográficas y de Cambio Climático, Instituto del Mar del Perú, Callao. Peru.

Correspondence to: Marco Yseki (marco.yseki@gmail.com)

Abstract. Reconstructing precipitation and wind from the geological record could help to understand the potential changes in precipitation and wind dynamics in response to climate change in Peru. The last deglaciation offers natural experimental conditions to test precipitation and wind dynamics response to high-latitude forcing. While considerable research has been done to reconstruct precipitation variability during the last deglaciation in the Atlantic sector of South America, the Pacific sector of South America has received little attention. This work aims to fill this gap by reconstructing types of terrigenous transport to the central-southern Peruvian margin (12°S and 14ºS) during the last deglaciation (18-13 kyr BP). For this purpose, we used grain-size distribution in sediments of marine core M77/2-005-3 (Callao, 12°S) and G14 (Pisco, 14ºS). We analyzed end-members (EMs) to identify grain-size components and reconstruct potential sources and transport processes of terrigenous material across time. We identified four end-members for both Callao and Pisco sediments. In Callao, we propose that the changes in the contributions of EM4 (101 μm) and EM2 (58 μm) mainly reflect the hydrodynamic energy and diffuse sources, respectively, while the variations in EM3 (77 μm) and EM1 (11 μm) reflect changes in the aeolian and fluvial inputs, respectively. In Pisco, where there are strong winds and extensive coastal desert, changes in the contribution of EM1 (10 μm) reflect changes in river inputs while EM2 (52 μm), EM3 (75 μm) and, EM4 (94 μm) reflect an aeolian origin. At millennial-scale, our record shows an increase of the fluvial inputs during the last part of Heinrich Stadial 1 (~ 16-14.7 kyr BP) at both locations. This increase was linked to higher precipitation in Andes related to a reduction of the Atlantic Meridional Overturning Circulation and meltwater discharge in North Atlantic. In contrast, during Bølling-Allerød interstadial (~ 14.7-13 kyr BP), there was an aeolian input increase, associated with stronger winds and lower precipitation that indicate an expansion of the South Pacific Subtropical High. These conditions would correspond to a northern displacement of the Intertropical Convergence Zone-South Subtropical High system associated with a stronger Walker circulation. Our results suggest that variations in river discharge and changes in surface wind intensity in the western margin of South America during the last deglaciation were sensitive to Atlantic Meridional Overturning Circulation variations and Walker circulation on millennial

34 timescales. In the context of global warming, large-scale increases in precipitation and fluvial discharge in the Andes as a
35 result of declining of Atlantic Meridional Overturning Circulation and southward displacement of the Intertropical
36 Convergence Zone should be considered.

1. Introduction

38 The last deglaciation, a period of global warming starting at the end of the Last Glacial Maximum (LGM, ~ 19 kyr BP) to the
39 Early Holocene (11.7 kyr BP), is an outstanding period in the earth's history that provides a better understanding of the
40 mechanisms regulating regional climatic conditions as a consequence of global warming (Clark et al., 2012; Shakun et al.,
41 2012). During the last deglaciation, variations in the meltwater discharge in the North Atlantic and their consequent impact on
42 the intensity of the Atlantic Meridional Overturning Circulation (AMOC) resulted in abrupt climatic changes on a millennial-
43 scale (McManus et al., 2004; Mulitza et al., 2017; Ng et al., 2018), which in turn caused changes in the meridional-oceanic
44 temperature gradient as well as a meridional shift of the mean annual position of the Intertropical Convergence Zone (ITCZ)
45 (Cheng et al., 2012; Deplazes et al., 2013; Mcgee et al., 2014).
46 Numerous studies based on both continental and marine records have evaluated the effects of meltwater discharge and
47 temperature variations in the North Atlantic on precipitation in Tropical South America (TSA) (e.g., Mollier-Vogel et al.,
48 2013; Novello et al., 2017; Mulitza et al., 2017; Stríkis et al., 2015, Bahr et al., 2018). Most such studies have suggested wetter
49 conditions in this region during cold events in the North Hemisphere, including the Heinrich Stadial 1 (HS1, ~ 18-14.7 kyr
50 BP) and the Younger Dryas (YD, ~ 12.9-11 kyr BP). This has been linked to a southern displacement of the ITCZ (e.g.,
51 Mollier-Vogel et al., 2013; Mulitza et al., 2017; Bahr et al., 2018) and an intensification of the South American Monsoon in
52 its southern domain (Novello et al., 2017; Stríkis et al., 2015) in response to the weakening of the AMOC and increased
53 meltwater discharges into the North Atlantic. Conversely, during the Bølling-Allerød (B-A, 14.7-12.9 kyr BP), a warm period
54 in the North Hemisphere, dry conditions developed in TSA (e.g., Mollier-Vogel et al., 2013; Novello et al., 2017; Mulitza et
55 al., 2017) due to the strong AMOC, the more northerly position of the ITCZ, and the weakening of the South American
56 Monsoon.
57 However, most records covering the last deglaciation concern Eastern South America (e.g., Cruz et al., 2005; Montade et al.,
58 2015; Stríkis et al., 2015; Zhang et al., 2015; Novello et al., 2017, Mulitza et al., 2017; Bahr et al., 2018; Stríkis et al., 2018),
59 while records from the western slope of the Andes (e.g., Baker et al., 2001a, 2001b) and the Peruvian margin are scarce (e.g.,
60 Rein et al., 2005; Mollier-Vogel et al., 2013). Previous attempts to reconstruct changes in the precipitation in the western flank
61 of the Andes using marine sediment records have given rise to contrasting results. In Northern Peru (4ºS), based on titanium
62 (Ti) to calcium (Ca) ratios, Mollier-Vogel et al. (2013) suggest an increase in fluvial inputs during the HS1 and YD and reduced
63 precipitation during the B-A. However, off Callao (12ºS), no difference in fluvial inputs, here based on lithic content, between
64 HS1 and BA is reported (Rein et al., 2005). The difference between the two records could be because of the changes in sediment
65 transport at the two sites and/or to the interpretation of the proxies used in these studies. In both studies, Ti/Ca ratio at 4ºS

2

66 (Mollier-Vogel et al., 2013) and lithic content at 12ºS (Rein et al., 2005) were considered as indicators of the fluvial inputs.

67 The latter, is generally true in Northern Peru (4ºS) where rainfall can reach 466 mm y^{-1} (Lagos et al., 2008). However, other

68 processes can be invoked in more arid regions, for example, in central-southern Peru where rainfall is scarce (less than 20 mm

69 y^{-1}) (Lagos et al., 2008). Indeed, Briceño-Zuluaga et al. (2016) have shown that, during the last millennium, part of the detrital

70 fraction of marine sediments collected off Pisco was also of aeolian origin. According to Briceño-Zuluaga et al. (2016) aeolian

71 inputs off Pisco can contribute up to almost 50% of the terrigenous fraction during some climatic periods (e.g., the Medieval

72 Climatic Anomaly). These results are based on the grain size distributions of terrigenous components in the sediment.

73 The grain-size distribution of Peruvian margin sediments is typically polymodal, and for this reason, it can information on

74 sediment transport mechanisms and/or sediment sources (Briceño-Zuluaga et al., 2016). Aeolian particles diameters are

75 relatively coarser than fluvial ones and if wind intensification occurs, the aeolian flow and the frequency of coarse particles (~

76 >36 μm) would increase. Thus, the relative abundance of fluvial particles (~ 6-14 μm) would reflect the precipitation and

77 continental runoff (e.g., Stuut et al., 2002; Stuut and Lamy 2004; Pichevin et al., 2005; Briceño-Zuluaga, et al., 2016; Beuscher

78 et al., 2017). Mathematical methods can be to identify the grain-size components of polymodal sediments. For instance, end-

79 member analysis (EMA) has been widely used to infer changes in fluvial and/or aeolian inputs (e.g., Stuut et al., 2002, 2004,

80 2007, 2014; Weltje y Prins, 2003; 2007; Pichevin et al., 2005; Holz et al., 2007; Just et al., 2012; Beuscher et al., 2017;

81 Humphries et al., 2017; Jiang et al., 2017).

82 The aim of the current work is to reconstruct at the millennial-scale the transport (fluvial and aeolian) and sedimentation of

83 the terrigenous inputs off central-southern Peru (Callao and Pisco) during the last deglaciation. To achieve this, grain size

84 distributions on surface sediments and sediments cores (M77/2-005-3, Callao and G14, Pisco) were measured and EMA was

85 used to deconvolved them into subpopulations. Surface sediments were collected during normal conditions and during the

86 2017 Coastal El Niño (April 2017). During the 2017 Coastal El Niño, the flow of the Callao and Pisco Rivers reached extremely

87 high levels during austral summer 2017, especially during March 2017 (Guzman et al., 2020). Likewise, in the month of April

88 2017, wind surface anomalies were positive, especially in Central and Southern Peru (Echevin et al., 2018). Chamorro et al.

89 (2018) found a quasi-linear relationship between surface wind and pressure gradient anomalies during the El Niño period in

90 1998. The alongshore pressure gradient anomalies, in 1998, were caused by a greater increase in near-surface air temperature

91 off the northern coast than off the southern coast of Peru. This inhomogeneous sea surface warming is similar during El Niño

92 2017. Based on the above, the samples collected in April 2017 may reflect changes in fluvial and maybe aeolian transport

93 associated with Coastal or East Pacific El Niño events.

94 In addition, as a proxy for fluvial vs aeolian inputs, we used the titanium/zirconium (Ti/Zr) record from X-Ray fluorescence

95 (XRF) analysis of the 106KL core collected off Callao and described by Rein et al. (2005). In a subsequent step, Ti, Al and Zr

96 were measured in surface sediments at Callao and Pisco by ICP-MS to better interpret the XRF results. We postulate that

97 changes in the AMOC intensity have modulated the variability of winds and precipitation in the Western TSA, as inferred by

98 changes in the grain-size distribution of marine sediment particles, at millennial time-scales. Our work provides new

99 information on sedimentation, types of transport and sources of terrigenous inputs on the Peruvian margin during the last

3

Eliminó:), the latter characterized by increased river discharges (Guzman et al., 2020) and variations of surface winds in Peru (Echevin et al., 2018). These observations allow us to understand the effect of changes in precipitation and winds on grain-size distribution during periods of different climatic conditions.

deglaciation, offering a better understanding of the mechanisms modulating these processes during past periods of global warming.

1.2 Regional setting

We focused on the central-southern part (12-14ºS) of the Peruvian margin. Callao and Pisco are located onshore in the Lima Basin (Suess et al., 1987). This basin exhibits high productivity and anoxic conditions that are favored by an intense oxygen minimum zone between about 200 and 400 meters depth (Cardich et al., 2019); hence, sediments are composed of fine grains, are rich in organic matter, and contain abundant diatoms. The general absence of bioturbation in some areas and during some time periods allows for the preservation of laminations and, therefore, their use as palaeoceanographic records (e.g., Rein et al., 2005; Gutiérrez et al., 2006, 2009, 2011; Sifeddine et al., 2008; Salvatteci et al., 2014a, 2016, 2019; Briceño-Zuluaga et al., 2016;). In Callao, muddy laminated areas are reported (Reinhardt et al., 2002), but sedimentary records collected in the OMZ core, off Pisco, show more continuous laminations than the records collected off Callao (e.g., Salvatteci et al., 2016, 2019).

The main transport of the detrital fraction of coarse silt and sand to the hemipelagic sediments in the Peruvian margin occurs by the action of winds (Scheidegger and Krissek, 1982). In contrast to Callao, Pisco is characterized by the presence of large coastal deserts, extreme aridity and dust storms known as Paracas winds. During these sporadic sand storms, wind velocities can exceed 10-15 m/s (Briceño-Zuluaga et al., 2017); these storms are produced by the local intensification of alongshore surface wind and by alongshore pressure gradients (Briceño-Zuluaga et al., 2017). Moreover, in Pisco, an intense coastal upwelling linked to strong alongshore surface wind occurs (Dewitte et al., 2011; Gutiérrez et al., 2011; Rahn and Garreaud, 2013). The intensity of alongshore surface winds presents a seasonal variability, with stronger winds during austral winter and weaker winds during austral summer (Fig. 1). This seasonality is linked regionally to the displacements of the ITCZ-South Pacific Subtropical High (SPSH) system and locally to continental-oceanic and alongshore pressure gradients (Strub et al., 1998; Gutiérrez et al., 2011; Chamorro et al., 2018). In contrast to the coarser particles that are transported by winds, quartz-rich silt and clays are transported by rivers to the continental shelf (Scheidegger and Krissek, 1982). The central-southern Peruvian coast is characterized by very low annual precipitations (Callao,14 mm y^{-1} and Pisco, 2 mm y^{-1}) and intermittent flows of coastal rivers (Lagos et al., 2008). However, during austral summer, there is an increase in river discharges associated with increased monsoon precipitation in the Andes (Garreaud et al., 2009; Vuille et al., 2012). Occasional floods occur and higher sediment discharges are associated with intense precipitation during extreme El Niño events (Bourrel et al., 2015; Morera et al., 2017; Rau et al., 2016; Guzman et al., 2020).

A large fraction of the particles smaller than 10 μm (desert aerosols) are transported beyond the continental shelf (Saukel et al., 2011). Therefore, the fine fraction of aeolian origin in the continental shelf sediments is therefore negligible, and the fine fraction of the continental shelf is largely dominated by fluvial inputs. On the other hand, coarser particles (e.g., > 40 μm) settle on the continental shelf (Scheidegger and Krissek, 1982). Once in the water column, the dispersion patterns of clays (< 4 μm) and fine silts (8-11 μm) coincide with the surface and subsurface currents, while the coarser fraction presents limited

Eliminó: large quantities of

Eliminó: Aeolian clays and silts are transported offshore by trade winds (Saukel et al., 2011),

141 dispersion near the coast (Scheidegger and Krissek, 1982). Likewise, near-bottom processes and bottom topography exert

142 considerable control over the dispersal of hemipelagic sediments on the Peruvian margin (Scheidegger and Krissek, 1982).

2. Materials and methods

2.1 Surface sediments, marine core and age model

145 Surface sediments (0-0.5 cm) were collected in front of Callao (N=12) and Pisco (N=9) at depths of 92-178 m and 120-311 m,

146 respectively, by the Instituto del Mar del Peru during the years 2015 (December), 2016 (August and December) and 2017

147 (February, April and, August), specifically along transects perpendicular to the coast (Fig. S1). Details of the sampling sites

148 are given in Table S1. The samples collected in April 2017 coincided with the occurrence of a Coastal El Niño event, and will

149 be considered as representative of "Coastal El Niño" conditions hereafter. All the other samples will represent "normal"

150 conditions.

151 The core M77/2-005-3, was retrieved from the Southeast Pacific continental slope (12º05 S, 77º40,07 W, 214 m water depth,

152 1336 cm long) during the M77-2 expedition in 2008 (Fig. 1). Because we focus on the last deglaciation period, we worked

153 with the section from 0 to 700 cm core depth. A first depth-age model based on four 14C ages was built by Salvatteci et al.

154 (2019). In the present, we added 22 ^{14}C ages and developed a new age depth-age model (Table S2). Radiocarbon measurements

155 were performed on organic matter at the Laboratoire de Mesures du Carbone-14 (LMC14, Gif-sur Yvette, France). Ortlieb et

156 al. (2011) reported a regional reservoir effect (ΔR) of 511 ± 278 years for the Early Holocene (10.4-6.8 kyr) and in the absence

157 of ΔR data for older periods, we used this value to calibrate the 14C measurements for the last deglaciation as in Salvatteci et

158 al. (2016, 2019). To construct the age model, we used the maximum probability ages obtained from the CALIB 8.1 software

159 using the Marine 20 dataset. The chronological model based on the lineal model indicates that the examined section (0-700

160 cm) of core M77/2-005-3 (Fig. S2) recorded the LGM and the last deglaciation (22-13 kyr BP; 95-700 cm). Core M77/2-005-

161 3 presents a hiatus at 94 cm, so a great part of the Holocene is missing.

162 Core G14 (14ºS, 76ºW, 390 m water depth) was retrieved during the Galathea-3 expedition in 2007 (Salvatteci et al., 2016).

163 The radiocarbon dates of G14 were published in Salvatteci et al. (2016). For the current study, a new depth-age model based

164 on a lineal model was developed with an updated calibration using the CALIB 8.1 software and the Marine 20 dataset. The

165 upper part of sediment layers was not recovered in G14, which ranges from 13.4 to 24.6 kyr BP (Fig. S2).

166 The lithological descriptions of M77/2-005-3 and G14 are available in Salvatteci et al. (2016, 2019). The M77/2-005-3 and

167 G14 cores show laminated and banded sediments with no evident signs of major discontinuities during the last deglaciation

168 (Salvatteci et al., 2016, 2019). The G14 core presents more continuous laminated sediments compared with the M722-005-3

169 core. (Salvatteci et al., 2016, 2019).

170 To compare our new data from cores M77/2-005-3 and G14 with previously published records in the area we modified the age

171 model of core 106 KL (Rein et al., 2005). Core 106 KL (12°030S, 77°39.80W, 184 m water depth) was retrieved during cruise

172 SONNE 147 (Rein et al., 2004, 2005). The chronology model and lithology have been fully described in Rein et al. (2004,

---

Eliminó: bulk

Eliminó: sediment

Eliminó: packaged

176 2005). A new depth-age model based on a lineal model was developed with an updated calibration using the CALIB 8.1

177 software and the Marine 20 dataset (Fig. S2) and we only used the sections covering the last deglaciation.

178
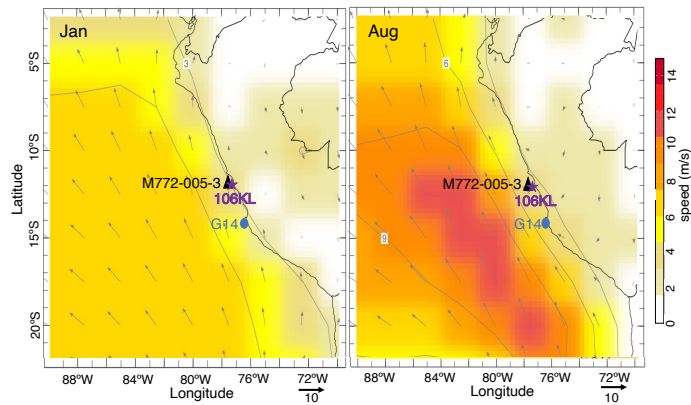
179

180 **Figure 1. (A) Location of the sampling of the sediment cores M77/2-005-3, 106Kl and G14 core. Average wind speed (m/s) at 1000**
181 **hPa in January and August (http://iridl.ldeo.columbia.edu).**

182

183 **2.2 Grain-size distribution and end-member analysis**

184 To reduce the effect of sediment disturbances that can produce artificial results, only laminated and banded sequences were

185 subsampled for grain-size distribution analysis. Reworked sediments are widespread in the marine sediment records off Peru

186 and can be distinguished from well-preserved sediments using X-ray images (Salvatteci et al., 2014b). For both surface and

187 core sediment samples, to isolate the terrigenous fraction, we followed the procedure described in Briceño-Zuluaga et al.

188 (2016). Organic matter, calcium carbonates and biogenic silica were successively removed with hydrogen peroxide (H_2O_2 30%

189 at 60ºC for 3 to 4 days), hydrochloric acid (HCl 10% for 12h), and sodium carbonate (Na_2CO_3, 1M at 90ºC for 3h), respectively.

190 The grain-size distribution was then measured using an automated image analysis system (model FPIA3000, Malvern

191 Instruments), here with a measurement range of 0.5-200 μm. Further details on the FPIA3000 are described in Flores-

192 Aqueveque et al. (2014) and Briceño-Zuluaga et al. (2016). Given that only particles smaller than 200 μm could be measured

193 under the analytical conditions applied in the present work, all samples were sieved with a 200 μm mesh before being analyzed.

194 Particles larger than 200 μm were not recovered in any sample; thus, our analysis covers the full range of grain size present in

195 the surface and cores sediments.

6

196 The grain-size distribution was generally plurimodal and for this reason we have used AnalySize modelling algorithm
197 (Paterson and Heslop, 2015), to deconvolute the grain-size distributions; the algorithm establishes a physical mixing model
198 that transforms the measured particle size distribution histograms into the sum of a limited number of end members (Ems)
199 with an unimodal particle size distribution. The sum of determination coefficients (r^2), which represent the proportion of the
200 variance of each EM against the total granulometric distribution, is calculated to estimate the minimum number of EMs
201 necessary to reach a high percentage of the total variance. More specific details are available in Paterson and Heslop (2015).

2.3 ICP-MS analysis

203 The Al, Ti, and Zr concentrations in the surface sediments were determined by inductively coupled plasma mass spectrometry
204 (ICP-MS) (Agilent 7500 cx) after hot-plate acid digestion in polytetrafluoroethylene (PTFE) vessels. The employed acids (HF,
205 HNO3, and HClO4) eliminated organic material and solubilized silicates (Jarvis et al., 1992). The complete protocol is
206 described in details in Salvatteci et al. (2014a). The accuracy of the concentration measurements was determined by
207 comparison with MESS-3 (Marine sediment reference material, National Research Council of Canada). The relative standard
208 deviation (RSD) estimated from duplicate analysis was less than 3.5 % for Al, Ti, and Zr.

2.4 XRF analysis

211 The piston core KL 106 was analyzed using an Avaatech XRF Core Scanner at the Marum Center (Bremen). Here, XRF
212 scanning was done for 19 elements at 2-mm intervals. Ti is an aluminum/silicate-related element and is associated mainly with
213 clay minerals transported from the continent to the ocean through river discharges (Jansen et al., 1998; Yarincik et al., 2000).
214 Conversely, Zr is predominantly enriched in heavy mineral species, in particularly zircon. The latter is broadly distributed in
215 natural sediments and typically has a relatively coarse grain size (Pettijohn, 1941). Zr has been widely used as a proxy for
216 mean depositional grain-size variations (e.g., Dypvik and Harris, 2001; Wu et al., 2020). Using the Ti/Zr ratio, we compared
217 Ti, which is present in all sizes of sediment, but especially in clays, to Zr, which would only be present in the silt and sand
218 fractions in the form of zircon minerals. Assuming that fine particles, such as clays, are mainly transported by rivers, while
219 coarse particles (coarse silts and sands) come mainly from an aeolian origin, the Ti/Zr ratio can be used as a potential proxy
220 for fluvial versus aeolian inputs.

3. Results

3.1 Grain-size distribution of the surface sediments

223 The grain-size distribution of all surface samples collected at the stations in Callao and Pisco are shown in Fig. 2. In Callao
224 and Pisco, during normal conditions, the abundance of fine particles (< 10 μm) was higher at the deepest and furthest offshore
225 stations than at coastal stations, while, coarse particles (60-120 μm) were more abundant close to the coast (Fig. 2). Coarser

7

particles <u>were</u> deposited mainly on the inner continental shelf <u>because of</u> their weight. During the 2017 Coastal El Niño, a strong increase in fine particles (< 10 μm) abundance was found only at station E2 (Fig. 2a) in Callao. On the other hand, the abundance of the coarse fraction (50-100 μm) in the sediments from the most distant stations (E12 and E11) increased in Pisco (Fig. 2d and 2e).
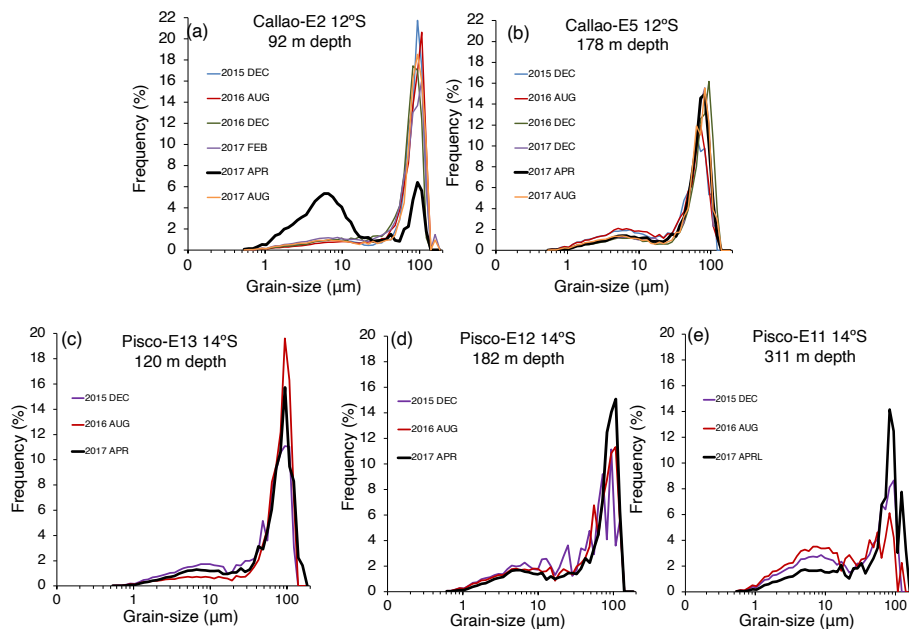
Figure 2. Grain-size distribution of surface sediments <u>at the</u> Callao (a, b) and Pisco stations (c, d, e).

The mean grain-size distribution per climatic period analyzed is shown in <u>Fig.</u> 3a and 3b. During the Late HS1 (16-14.7 kyr BP), the abundance of fine particles (< 10 μm) <u>was</u> higher than during the Early HS1 (18-16 kyr BP) and B-A in Callao and Pisco (Fig. 3a and 3b). This increase <u>was</u> more <u>pronounced</u> in Callao (Fig. 3a). On the other hand, during the B-A (14.7-13 kyr BP), the sediments <u>were</u> characterized by <u>a</u> high abundance of coarser particles (Fig 3a and 3b).
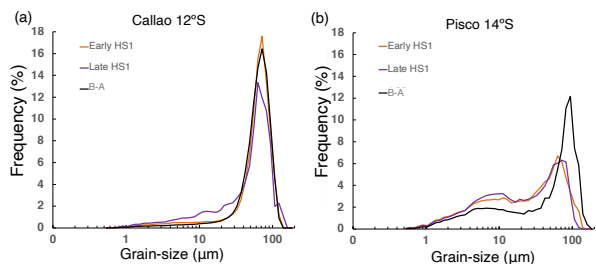
Figure 3. Mean grain-size distribution by climatic period in Callao (a) and Pisco (b).

3.2 End-member analysis

Based on a multiple correlation coefficient, a model with four EMs was chosen in Callao and Pisco, which explained 98% and 95% of the variance of the grain-size distribution data set, respectively (Fig. 4a and 4b). The measured and modeled grain-size distribution were highly correlated (R2: 0.86-0.99) for each analyzed sample, attesting to the fact that the use of four EMs was appropriate for our interpretation. Although a model with two EMs model explained 95% of the variance of the data in Callao, the variability of each EM's contribution was different (Fig. 6), suggesting that each EM indicated different processes or sources. Each of the four EMs presented a unimodal distribution, with its median being respectively at 11 μm (EM1), 58 μm (EM2), 77 μm (EM3) and 101 μm (EM4) in Callao (Fig. 4c). In Pisco, each EM was represented by a unimodal distribution centered at 10 μm (EM1), 52 μm (EM2), 75 μm (EM3) and 94 μm (EM4) (Fig. 4d).
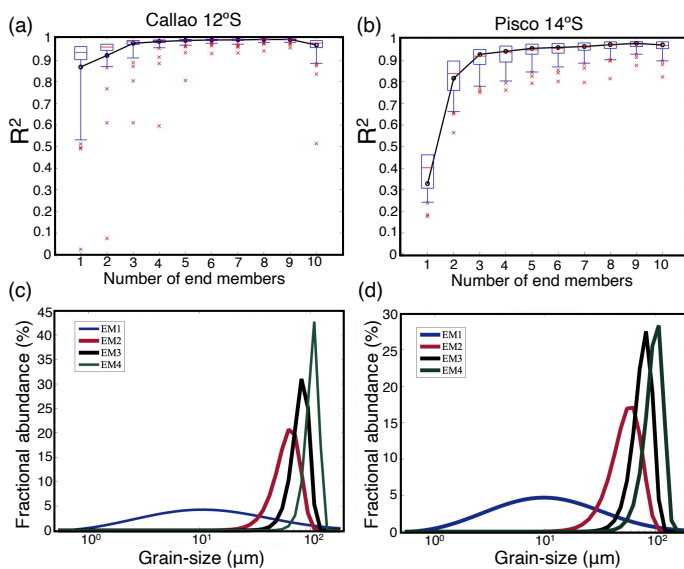
9

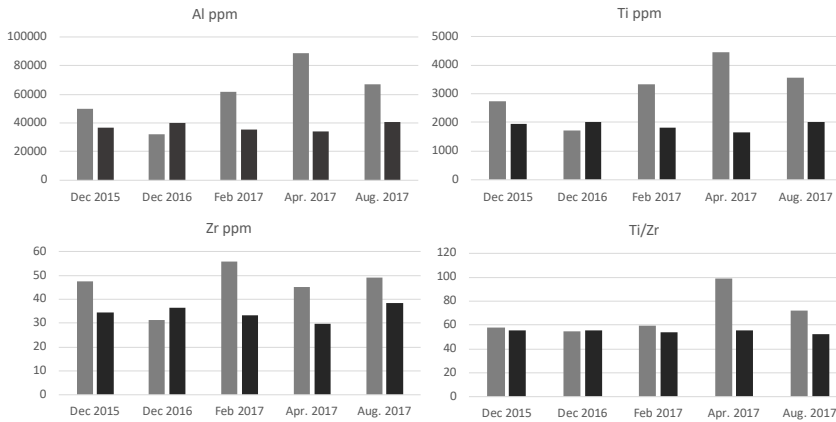Figure 4. Coefficient of determination (r2) as a function of the number of end members chosen to model the observed grain-size distribution in Callao (a) and Pisco (b). Grain size distribution of the four end-members in Callao (c) and Pisco (d).

3.3 ICP-MS and XRF analysis

The concentrations of Al, Ti, Zr, and Ti/Zr ratio of the surface samples collected at Callao are presented in Fig. 5. The E2 station in Callao showed a very large increase in Ti and Al during the Coastal El Niño (April 2017), with values twice the average of all other samples. This was related to the large amount of fine particles measured that month in Callao. Regarding Zr, no significant difference between normal conditions and Coastal El Niño was observed in E2 and E5 Callao. However, we found higher average Zr concentrations for E2 (46 ± 9 ppm) compared with for E5 (34 ± 3 ppm) because the E2 station was

10

closer to the coast and received more sandy inputs. Finally, the Ti/Zr ratio was 1.7 times higher during the Coastal El Niño (April 2017) with to normal conditions at E2.

Figure 5. Al, Ti, and Zr concentration values in ppm and Ti/Zr ratio of surface samples collected at Callao stations. Gray: E2 stations (92m depth), Black: E5 station (178m depth).

The Ti/Zr record of core 106Kl, Callao, used as a proxy for fluvial versus. aeolian inputs, shows millennial variability. During HS1, similar to the increment in fine particle abundance (Fig. 3a), Ti/Zr values were higher during late HS1 than during early HS1 (Fig. 7f). During B-A, a decreasing trend in Ti/Zr ratio was reported (Fig. 7f) by the increase in coarse particle abundance (Fig. 3a).

4. Discussion

4.1 Assignment of end-members

The terrigenous materials deposited on the Peruvian margin are transported by rivers and by wind activity, however, there are also other diffused sources like the material produced by coastal erosion transported offshore by marine currents. The terrigenous sediments in Callao and Pisco are multimodal which suggest that different processes are involved in the transport and deposition of these sediments. In both cores, we observed one end-member corresponding to a fine fraction (EM1) and three EMs corresponding to coarse fractions (EM2, EM3 and EM4). A previous study in Pisco used the variations of fine (10

11

305 µm) and coarse (50 µm and 100 µm) particles as proxies of river discharge and aeolian inputs respectively for the last few

306 centuries (Briceño-Zuluaga et al., 2016). However, the differences in the aeolian sources, shelf and slope morphology, currents

307 intensity, and hydrodynamics between Callao and Pisco, may modify the interpretation of the proxies described by Briceño-

308 Zuluaga et al. (2016).

309 EM1 showed a mode at 11 µm and 10 µm in Callao and Pisco, respectively, which is consistent with the grain-size of fine

310 particles (~ 6-14 µm) in marine sediments associated with river inputs reported in different areas of the world (e.g., Stuut and

311 Lamy, 2004; Stuut et al., 2007; Beuscher et al., 2017) and Pisco (Briceño-Zuluaga et al., 2016). Indeed, the increase of fine

312 particles (<10 µm) and EM1 contribution in the surface marine sediments from E2 Callao (Fig. 2a and Fig. 6a) associated with

313 local high fluvial discharges in Callao during the 2017 Coastal El Niño (Guzman et al., 2020) corroborates the use of variations

314 in the contribution of EM1 as an indicator of fluvial input changes. The no increase of fine particles (as well as Al and Ti

315 concentrations) in E5 Callao during Coastal El Niño was probably because of the greater distance between the fluvial source

316 and the sampling site.

317 Previous studies in the South Eastern Pacific used the abundance and fluxes of coarse particles (~ 36-100 µm) in marine

318 sediments as a proxy for wind intensity linked to the expansion/contraction of the SPSH (e.g., Flores-Aqueveque et al., 2015;

319 Briceño-Zuluaga et al., 2016). Based on HYSPLIT (Hybrid Single-Particle Lagrangian Integrated Trajectory) simulations,

320 Briceño-Zuluaga et al. (2017) have shown that coarse particles (50-90 µm) can directly reach the continental shelf in Pisco

321 during Paracas storms (characterized by wind velocities surpassing 10-15 m/s).

322 The EMs associated with the coarse fraction present similar modes in Callao and Pisco sediments (EM2, ~ 55 µm, EM3, ~ 75

323 µm and EM4, ~ 90-100 µm). Pisco is characterized by a large coastal desert and frequent dust storms. Also, because the shelf

324 at Pisco is narrow, the distance from terrestrial sources that can be transported by winds did not vary significantly during the

325 deglaciation compared with modern conditions. Based on this, particles between 50-90 µm (EM2, EM3 and EM4) can be

326 interpreted as indicators of aeolian input, as proposed by Briceño-Zuluaga et al. (2016). An increase in coarse particle

327 abundance in Pisco surface sediments was recorded at the stations most distant from the coast, E12 and E11, during April 2017

328 (Fig. 2d and 2e), when wind stress along the coast was anomalously enhanced, especially in Central and Southern Peru

329 (Echevin et al., 2018). This observation supports the hypothesis that these particles have an aeolian origin and that the increase

330 of their contribution suggests that, during events with stronger alongshore winds, these particles can be transported to a greater

331 distance than during normal conditions, modifying their proportion in the sediments, but because of t the small number of

332 samples, this variation was not statistically significant (Fig. 2d and 2e). Finally, although EM2, EM3 and EM4 reflected an

333 aeolian source, their contributions variations during the last deglaciation were different (Fig. 6b). This can possibly be

334 explained by changes in wind intensity; periods with stronger (weaker) winds result in an increase (decrease) in the amplitude

335 of coarser particles.

336 In Callao, the context is different because there are no large deserts near the coast and dust storms are rare, so is unlikely for

337 ~ 100 µm particles (EM4) to be transported directly to the sampling site. The presence of ~100 µm particles could possibly be

12

linked to bottom hydrodynamic processes. Indeed, during events of higher hydrodynamic energy, resuspension of fine particles and an increase in the relative frequency of coarser particles are expected. EM4 (101 µm) did not show drastic changes during the last deglaciation, suggesting that it did not influence the relative contribution of the other modes at the millennial-scale (Fig. 6a). EM2 (58 µm) was found to be the dominant mode in Callao, ranging from 40 to 80% (Fig. 6a). Although these coarse sediments can be transported by winds (Briceño-Zuluaga et al., 2016, 2017), it is unlikely that this high percentage of coarse particles could be transported solely by the wind directly to the sampling site off Callao. It is more likely that ~ 58 µm particles were derived from different sources (winds, coastal erosion) and are distributed on the continental shelf by the Peru-Chile Undercurrent (Reinhardt et al., 2002). In summary, based on the distance of the sampling site from the aeolian sources, in addition to the absence of large aeolian sources and dust storms in Callao, we propose that the changes in the contribution of EM2 and EM4 can be related mainly with other processes associated with diffuse sources and hydrodynamic energy respectively. Conversely, EM3 can be seen as the best proxy of a wind source.
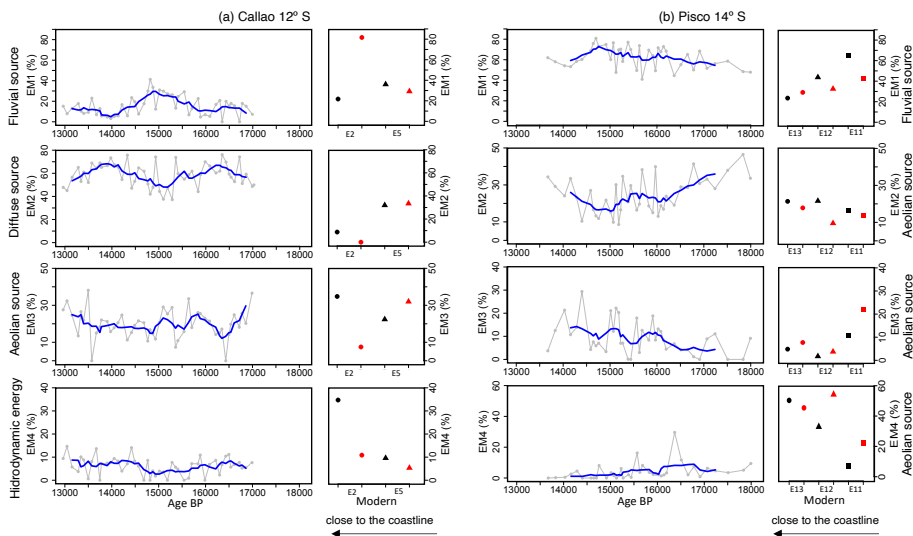
Figure 6. Variations in the contribution of the grain size end-members from marine cores and surface sediments in Callao (a) and Pisco (b). The modern period is represented by the mean end-member contribution of surface sediments collected during normal conditions (black symbols) and Coastal El Niño April 2017 event (red symbols).

13

4.2. Millennial variability of fluvial and aeolian inputs during the last deglaciation

The analysis of EMs allowed for a quantification of the main granulometric modes; however, because the sum of the contribution of the modes corresponds to 100%, it is difficult to consider the modes individually because an increase of one may reduce the others and influence their contribution variability. Thus, for a better visualization, a ratio between Ems indicative of a fluvial (EM1 in Callao and Pisco) and aeolian (EM3 in Callao and the sum of EM2, EM3 and EM4 in Pisco) source will be used as a proxy of the variations in the fluvial and aeolian inputs.

An increase in fluvial inputs based on the grain-size and EMA was observed during the Late HS1 (~16-14.7 kyr BP) with maximum values between ~15.5 kyr BP and 14.7 kyr BP in Callao (M77/2-005-3) and Pisco (G14) (Fig. 7g and 7h).

Likewise, the Ti /Zr record in Callao (106KL) indicated an increase in fluvial input during HS1, with maximum discharges between ~15.5 kyr BP and 14.9 kyr BP. The increment of Ti in surface sediments during higher fluvial discharges at Callao combined with the good relationship between the Ti/Zr record and the fluvial/aeolian record (EM1/EM3) during the last deglaciation in Callao can support the idea that Ti, which is mostly linked to the fine fraction of marine sediments, is mainly transported by rivers to the Peruvian margin and can be used as a proxy of river discharge and precipitation (e.g., Mollier-Vogel et al., 2013; Salvatteci et al., 2014; Fleury et al., 2015).

The contrasting differences between our record of fluvial input (based on grain size and Ti/Zr) and the record of lithic content based on reflectance (Rein et al., 2005) in Callao can be explained by the difference in the methodology and interpretation of the proxies. Rein et al. (2005) interpret the lithic content as a proxy for river discharges; however, as observed in our data (Fig. 6) and the literature (Briceño-Zuluaga et al., 2016), the terrigenous material can be transported to the central-southern Peruvian margin by different sources (e.g., fluvial and aeolian) and the variability of fluvial and aeolian transport follows different patterns, hence responding to different forcing.

Because heavy precipitation associated with the El Niño events in the Callao and Pisco coastal regions are occasional, a larger average fluvial discharge in Callao and Pisco would likely be related to precipitation fluctuations at higher elevations in the watersheds, in the Andes. Previous studies suggest a correlation between North Atlantic cooling and massive meltwater discharges with increased precipitation in the Central Andes (Baker et al., 2001a, 2001b; Blard et al., 2011, Martin et al., 2018; González-Pinilla et al., 2021). During the last deglaciation, cooling in the North Atlantic and higher meltwater discharges generated a weakening of the AMOC (MacManus et al., 2004; Mulitza et al., 2017; Ng et al., 2018). The latter generated an interhemispheric temperature contrast and an impact on precipitation in the Central Andes associated with a southward shift of the ITCZ and an intensification of the South American Monsoon in different regions: Central Andes (Baker et al., 2001a, 2001b; Blard et al., 2011; González-Pinilla et al. 2021), Southeast (Cruz et al. 2005; Stríkis et al., 2015) and Southwest Brazil (Novello et al., 2017) and in Western Amazonia (Sublette Mosblech et al., 2012; Cheng et al., 2013). Indeed, the higher river discharges we evidenced in Callao and Pisco during Late HS1 (~16-14.7 kyr BP) occurred simultaneously with the well-dated highstand of the giant paleolake Tauca (~16.6-14.5 kyr BP) (Martin et al., 2018). Therefore, the increase and decrease in river

14

416 discharges in central Peru during HS1 and B-A, respectively, could be explained by changes in precipitation in the Andes in
417 response to changes in the intensity of the AMOC and meltwater pulses in the North Atlantic.
418 During the past few decades, the ITCZ in the East Pacific has shifted southward in and generally narrowed and strengthened
419 (Zhou et al., 2020). A recent study suggests a narrowing and southward shift of the ITCZ in the Eastern Pacific in response to
420 the SSP3-7.0 scenario by 2100 (Mamalakis et al., 2021). Although there are uncertainties about the effects of current global
421 warming on AMOC intensity, there is evidence of the AMOC slowing over the past century (Rahmstorf et al., 2015; Caesar
422 et al., 2018) and in climate model simulations of future climate change, the AMOC is projected to decline generating a
423 southward displacement of the ITCZ (Bellomo et al., 2021). In the context of global warming, a large-scale precipitation and
424 fluvial discharge increases in Peru related to AMOC decline and southward displacement of the ITCZ should be considered.
425
426 Concerning the variations in the aeolian inputs and surface wind intensity in the Peruvian margin, changes in the intensity of
427 Walker circulation and meridional displacements of the ITCZ-SPSH system have been proposed as mechanisms to regulate
428 surface alongshore winds and upwelling dynamics in the Humboldt Current System at multiple timescales (e.g., Gutiérrez et
429 al., 2009; Briceño-Zuluaga et al., 2016; Salvatteci et al., 2014, 2019). On centennial timescales, a northern displacement of the
430 SPSH-ITCZ, here response to stronger Walker circulation, will an increase of alongshore winds and upwelling in Central-
431 South Peruvian margin (Salvatteci et al., 2014; Briceño-Zuluaga et al., 2016). An SST gradient increase in the equatorial
432 Pacific indicates a more intense Walker circulation in B-A than during HS1 (Fig. 8a) (Koutavas and Joanides, 2012). Moreover,
433 a northern displacement of the ITCZ has also been recorded during B-A. (Peterson et al., 2000; Deplazes et al., 2013). These
434 conditions should have provoked an increase of the alongshore winds and aeolian supply in central Peru during B-A. Indeed,
435 in Callao and Pisco, the aeolian inputs were the main transport from 14.7 to 13 kyr BP, suggesting, at least at the regional-
436 scale, an increase of alongshore wind and upwelling in Central-South Peru and an expansion of the SPSH (Fig. 8d and 8e).
437 Our record of surface wind intensity variations and an alkenone-derived SST reconstruction based on alkenones (Salvatteci et
438 al., 2019) in the same core collected from Callao showed similar trends (Fig. 8c). During HS1, a short cooling event between
439 16 and 15.5 kyr BP, coincided with stronger alongshore winds (Fig. 8c and d). And, during the B-A, a cooling at 14.7-13 kyr
440 BP, stronger aeolian transport associated with more intense alongshore winds occurred (Fig. 8c and 8d). These observations
441 suggest that local processes as upwelling variations in response to changes in alongshore wind intensity may control SST
442 variations during the last deglaciation, in addition to other processes such as the advection of the Southern Ocean and Antarctic
443 climate signals by the Humboldt Current.
444

**Eliminó:** SST proxies indicate an indicate an increase of the zonal

446
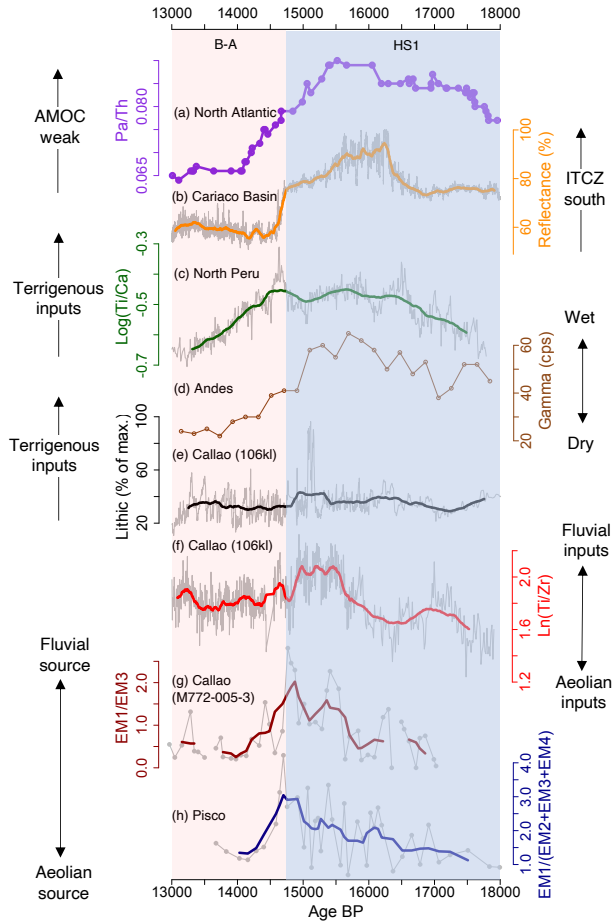
Figure 7. (a) Composite 231Pa/230Th record that reflect past changes in AMOC (Ng et al., 2018). (b) Reflectance (%) from Cariaco Basin as a proxy for the latitudinal displacement of the ITCZ (Deplazes et al., 2013). (c) Log (Ti/Ca) for core M77/2-059 from Northern Peru (4° S) (Mollier-Vogel et al., 2003). (d) Natural γ-radiation as a proxy for effective moisture in the Tropical Andes (Baker et al., 2021b). (e) Relative concentration of lithics for core 106Kl from Callao (Rein et al, 2005). (f) Ln (Ti/Zr) as a proxy for fluvial vs. aeolian inputs in core 106KL from Callao (this study). (g) EM1/EM2 ratio as a proxy for fluvial and aeolian source in Callao (this study). (h) EM1/(EM2+EM3+EM4) ratio as a proxy for fluvial and aeolian sources in Pisco (this study).

Eliminó: Callao

16

454
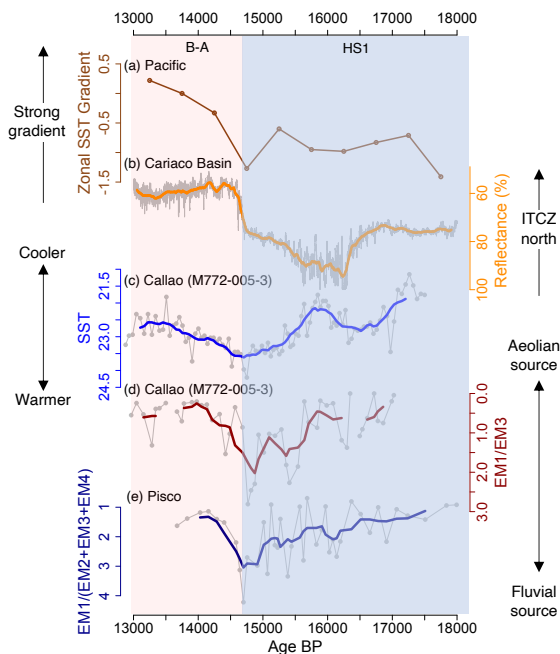
455
456 **Figure 8. (a) Zonal SST gradient anomaly during the last deglaciation, here calculated as the difference between Western and**
457 **Eastern Pacific averages (Koutavas and Joanides, 2012). (b) Reflectance (%) from the Cariaco Basin as a proxy for the latitudinal**
458 **displacement of the ITCZ (Deplazes et al., 2013). (c) Alkenone-derived near surface temperature from M77/2-005-3 core, Callao**
459 **(Salvatteci et al., 2019). (d) EM1/EM2 ratio (Reversal scale) as a proxy for fluvial and aeolian source in Callao (this study). (e)**
460 **EM1/(EM2+EM3+EM4) ratio (Reversal scale) as a proxy for fluvial and aeolian sources in Pisco (this study).**

461 **5. Conclusion**

462 The variability of the grain size distribution of marine sediments from the central-southern Peruvian margin (12ºS and 14ºS)

463 reveals millennial-scale changes in the transport and sedimentation processes of the terrigenous material during the last

464 deglaciation (18-13 kyr BP). We identified four granulometric EMs for both Callao and Pisco sediments, each of them

465 reflecting different processes and sources and whose interpretation must take into consideration regional contexts. In the case

466 of the Pisco core, located within the range of the aeolian inputs, as it has been shown earlier, the modes (EM2 to EM4)

467 corresponded to aeolian origin. In the case of the Callao core, which was located further from the coast and where sources of

17

eolian particles are scarce, the EM2 and EM4 modes have been interpreted as reflecting local hydrodynamics, while EM3 represented the eolian supply. Our results support a tight relationship between high latitude forcing and precipitation in the western flank of the Andes during the last deglaciation. During late HS1 (16-15 kyr BP), enhanced fluvial inputs in Callao and Pisco occurred and were associated with higher precipitation in the Central Andes in response to the slowdown of AMOC and meltwater discharge in the North Atlantic. Finally, the increase in the aeolian input during the B-A, could be a result of stronger alongshore winds linked to a northern displacement of the ITCZ-SPSH system in response to a strong gradient of the Walker circulation. There is still uncertainty about the effects of current climate change; however, there is evidence of a slowing of the AMOC over the past century and in future climate model simulations. In the latter, the decline in the AMOC is accompanied by a southward shift in the ITCZ. Thus, we can probably expect an increase in precipitation and river flow in Peru in the future.

Data availability

The data associated with this manuscript will be submitted in the PANGAEA database upon publication of this paper.

Author contributions

MY, BT and DG designed the study. MY and SC carried out the grain-size analysis. DG and GS conducted the XRF analysis of core KL 106. FV collected the surficial sample, prepared them and contributed to their interpretation. MY wrote the manuscript with the help of BT and SC. All authors discussed and commented on the paper.

Competing interests

The authors declare that they have no conflict of interests.

References

500

501 Bahr, A., Hoffmann, J., Schönfeld, J., Schmidt, M., Nürnberg, D., Batenburg, S. and Voigt, S.: Low-latitude expressions of
502 high-latitude forcing during Heinrich Stadial 1 and the Younger Dryas in northern South America, Global and Planetary
503 Change, 160, 1-9, doi:10.1016/j.gloplacha.2017.11.008, 2018.

504 Baker, P. A., Seltzer, G. O., Fritz, S. C., Dunbar, R. B., Grove, M. J., Tapia, P. M., Cross, S. L., Rowe, H. D. and Broda, J. P:
505 The History of South American Tropical Precipitation for the Past 25,000 Years. Science, 291(5504), 640–643,
506 doi:10.1126/science.291.5504.640, 2001a.

507 Baker, P., Rigsby, C., Seltzer, G., Fritz, S., Lowenstein, T., Bacher, N. and Veliz, C.: Tropical climate changes at millennial
508 and orbital timescales on the Bolivian Altiplano, Nature, 409(6821), 698-701, doi:10.1038/35055524, 2001b.

509 Blard, P., Sylvestre, F., Tripati, A., Claude, C., Causse, C., Coudrain, A., Condom, T., Seidel, J., Vimeux, F., Moreau, C.,
510 Dumoulin, J. and Lavé, J.: Lake highstands on the Altiplano (Tropical Andes) contemporaneous with Heinrich 1 and the
511 Younger Dryas: new insights from 14C, U–Th dating and δ18O of carbonates, Quaternary Science Reviews, 30(27-28), 3973-
512 3989, doi:10.1016/j.quascirev.2011.11.001, 2011.

513 Beuscher, S., Krüger, S., Ehrmann, W., Schmiedl, G., Milker, Y., Arz, H. and Schulz, H.: End-member modelling as a tool for
514 climate   reconstruction—An   Eastern   Mediterranean   case   study,   PLoS   ONE,   12(9),   e0185136,
515 doi:10.1371/journal.pone.0185136, 2017.

516 Bellomo, K., Angeloni, M., Corti, S. and von Hardenberg, J.: Future climate change shaped by inter-model differences in
517 Atlantic meridional overturning circulation response, Nature Communications, 12(1), doi:10.1038/s41467-021-24015-w,
518 2021.

519 Bourrel, L., Rau, P., Dewitte, B., Labat, D., Lavado, W., Coutaud, A., Vera, A., Alvarado, A. and Ordoñez, J.: Low-frequency
520 modulation and trend of the relationship between ENSO and precipitation along the northern to centre Peruvian Pacific coast,
521 Hydrological Processes, 29(6), 1252-1266, doi:10.1002/hyp.10247, 2014.

522 Briceño-Zuluaga, F. J., Sifeddine, A., Caquineau, S., Cardich, J., Salvatteci, R., Gutierrez, D., Ortlieb, L., Velazco, F., Boucher,
523 H. and Machado, C.: Terrigenous material supply to the Peruvian central continental shelf (Pisco, 14° S) during the last 1000
524 years: paleoclimatic implications, Clim. Past, 12(3), 787–798, doi:10.5194/cp-12-787-2016, 2016.

525 Briceño-Zuluaga, F., Castagna, A., Rutllant, J. A., Flores-Aqueveque, V., Caquineau, S., Sifeddine, A., Velazco, F., Gutierrez,
526 D. and Cardich, J.: Paracas dust storms: Sources, trajectories and associated meteorological conditions, Atmospheric
527 Environment, 165, 99–110, doi:10.1016/j.atmosenv.2017.06.019, 2017.

528 Caesar, L., Rahmstorf, S., Robinson, A., Feulner, G. and Saba, V.: Observed fingerprint of a weakening Atlantic Ocean
529 overturning circulation, Nature, 556(7700), 191-196, doi:10.1038/s41586-018-0006-5, 2018.

530 Chamorro, A., Echevin, V., Colas, F., Oerder, V., Tam, J. and Quispe-Ccalluari, C.: Mechanisms of the intensification of the
531 upwelling-favorable winds during El Niño 1997–1998 in the Peruvian upwelling system, Climate Dynamics, 51(9-10), 3717-
532 3733, doi:10.1007/s00382-018-4106-6, 2018.

19

533 Cheng, H., Sinha, A., Cruz, F., Wang, X., Edwards, R., d'Horta, F., Ribas, C., Vuille, M., Stott, L. and Auler, A.: Climate
534 change patterns in Amazonia and biodiversity, Nature Communications, 4(1), doi:10.1038/ncomms2415, 2013.

535 Cheng, H., Sinha, A., Wang, X., Cruz, F. W. and Edwards, R. L.: The Global Paleomonsoon as seen through speleothem
536 records from Asia and the Americas, Clim Dyn, 39(5), 1045–1062, doi:10.1007/s00382-012-1363-7, 2012.

537 Clark, P. U., Shakun, J. D., Baker, P. A., Bartlein, P. J., Brewer, S., Brook, E., Carlson, A. E., Cheng, H., Kaufman, D. S. and
538 Liu, Z.: Global climate evolution during the last deglaciation, Proceedings of the National Academy of Sciences, 109(19),
539 E1134–E1142, doi:10.1073/pnas.1116619109, 2012.

540 Cruz, F. W., Burns, S. J., Karmann, I., Sharp, W. D., Vuille, M., Cardoso, A. O., Ferrari, J. A., Silva Dias, P. L. and Viana,
541 O.: Insolation-driven changes in atmospheric circulation over the past 116,000 years in subtropical Brazil, Nature, 434(7029),
542 63–66, doi:10.1038/nature03365, 2005.

543 Deplazes, G., Lückge, A., Peterson, L. C., Timmermann, A., Hamann, Y., Hughen, K. A., Röhl, U., Laj, C., Cane, M. A. and
544 Sigman, D. M.: Links between tropical rainfall and North Atlantic climate during the last glacial period, Nature Geosci, 6(3),
545 213–217, doi:10.1038/ngeo1712, 2013.

546 Dewitte, B., Illig, S., Renault, L., Goubanova, K., Takahashi, K., Gushchina, D., Mosquera, K. and Purca, S.: Modes of
547 covariability between sea surface temperature and wind stress intraseasonal anomalies along the coast of Peru from satellite
548 observations (2000–2008), Journal of Geophysical Research, 116(C4), doi:10.1029/2010jc006495, 2011.

549 Dypvik, H. and Harris, N.: Geochemical facies analysis of fine-grained siliciclastics using Th/U, Zr/Rb and (Zr+Rb)/Sr ratios,
550 Chemical Geology, 181(1-4), 131-146, doi:10.1016/s0009-2541(01)00278-9, 2001.

551 Echevin, V., Colas, F., Espinoza-Morriberon, D., Vasquez, L., Anculle, T. and Gutierrez, D.: Forcings and Evolution of the
552 2017 Coastal El Niño Off Northern Peru and Ecuador, Frontiers in Marine Science, 5, doi:10.3389/fmars.2018.00367, 2018.

553 Fleury, S., Martinez, P., Crosta, X., Charlier, K., Billy, I., Hanquiez, V., Blanz, T. and Schneider, R. R.: Pervasive multidecadal
554 variations in productivity within the Peruvian Upwelling System over the last millennium, Quat. Sci. Rev., 125, 78–90,
555 doi:10.1016/j.quascirev.2015.08.006, 2015.

556 Flores-Aqueveque, V., Alfaro, S., Vargas, G., Rutllant, J. A. and Caquineau, S.: Aeolian particles in marine cores as a tool for
557 quantitative high-resolution reconstruction of upwelling favorable winds along coastal Atacama Desert, Northern Chile, Prog.
558 Oceanogr., 134, 244–255, doi:10.1016/j.pocean.2015.02.003, 2015.

559 Flores-Aqueveque, V., Caquineau, S., Alfaro, S., Valdes, J. and Vargas, G.: Using Image-Based Size Analysis For Determining
560 the Size Distribution and Flux of Eolian Particles Sampled In Coastal Northern Chile (23 S), Journal of Sedimentary Research,
561 84(4), 238-244, doi:10.2110/jsr.2014.23, 2014.

562 Garreaud, R., Vuille, M., Compagnucci, R. and Marengo, J.: Present-day South American climate, Palaeogeography,
563 Palaeoclimatology, Palaeoecology, 281(3-4), 180-195, doi:10.1016/j.palaeo.2007.10.032, 2009.

564 González-Pinilla, F., Latorre, C., Rojas, M., Houston, J., Rocuant, M., Maldonado, A., Santoro, C., Quade, J. and Betancourt,
565 J.: High- and low-latitude forcings drive Atacama Desert rainfall variations over the past 16,000 years, Science Advances,
566 7(38), doi:10.1126/sciadv.abg1333, 2021.

567 Gutiérrez, D., Bouloubassi, I., Sifeddine, A., Purca, S., Goubanova, K., Graco, M., Field, D., Méjanelle, L., Velazco, F., Lorre,

568 A., Salvatteci, R., Quispe, D., Vargas, G., Dewitte, B. and Ortlieb, L.: Coastal cooling and increased productivity in the main

569 upwelling zone off Peru since the mid-twentieth century, Geophys. Res. Lett., 38(7), doi:10.1029/2010GL046324, 2011.

570 Gutiérrez, D., Sifeddine, A., Field, D., Ortlieb, L., Vargas, G., Chávez, F., Velazco, F., Ferreira, V., Tapia, P., Salvatteci, R.,

571 Boucher, H., Morales, M., Valdés, J., Reyss, J., Campusano, A., Boussafir, M., Mandeng-Yogo, M., García, M. and

572 Baumgartner, T.: Rapid reorganization in ocean biogeochemistry off Peru towards the end of the Little Ice Age,

573 Biogeosciences, 6(5), 835-848, doi:10.5194/bg-6-835-2009, 2009.

574 Gutiérrez, D., Sifeddine, A., Reyss, J. L., Vargas, G., Velazco, F., Salvatteci, R., Ferreira, V., Ortlieb, L., Field, D.,

575 Baumgartner, T., Boussafir, M., Boucher, H., Valdés, J., Marinovic, L., Soler, P. and Tapia, P.: Anoxic sediments off Central

576 Peru record interannual to multidecadal changes of climate and upwelling ecosystem during the last two centuries, Adv.

577 Geosci., 6, 119–125, doi:10.5194/adgeo-6-119-2006, 2006.

578 Guzman, E., Ramos, C. and Dastgheib, A.: Influence of the El Niño Phenomenon on Shoreline Evolution. Case Study: Callao

579 Bay, Perú, Journal of Marine Science and Engineering, 8(2), 90, doi:10.3390/jmse8020090, 2020.

580 Haug, G., Hughen, K., Sigman, D., Peterson, L. and Röhl, U.: Southward Migration of the Intertropical Convergence Zone

581 Through the Holocene, Science, 293(5533), 1304-1308, doi:10.1126/science.1059725, 2001.

582 Holz, C., Stuut, J. B. W., Henrich, R. and Meggers, H.: Variability in terrigenous sedimentation processes off northwest Africa

583 and its relation to climate changes: Inferences from grain-size distributions of a Holocene marine sediment record, Sediment.

584 Geol., 202(3), 499–508, doi:10.1016/j.sedgeo.2007.03.015, 2007.

585 Humphries, M. S., Benitez-Nelson, C. R., Bizimis, M. and Finch, J. M.: An aeolian sediment reconstruction of regional wind

586 intensity and links to larger scale climate variability since the last deglaciation from the east coast of southern Africa, Global

587 and Planetary Change, 156, 59–67, doi:10.1016/j.gloplacha.2017.08.002, 2017.

588 Jansen, J., Van der Gaast, S., Koster, B. and Vaars, A.: CORTEX, a shipboard XRF-scanner for element analyses in split

589 sediment cores, Marine Geology, 151(1-4), 143-153, doi:10.1016/s0025-3227(98)00074-7, 1998.

590 Jarvis, K. E., A. L. Gray, and R. S. Houk. Handbook of Inductively Coupled Plasma Mass Spectrometry. Blackie Academic

591 & Professional, an imprint of Champan & Hall, Wester Cleddens Road, Bishopgriggs, Glasgow, London Glasgow New York

592 Tokyo Merlbourne Madras, 1992.

593 Jiang, H., Zhong, N., Li, Y., Ma, X., Xu, H., Shi, W., Zhang, S. and Nie, G.: A continuous 13.3-ka record of seismogenic dust

594 events in lacustrine sediments in the eastern Tibetan Plateau, Sci Rep, 7(1), doi:10.1038/s41598-017-16027-8, 2017.

595 Just, J., Heslop, D., von Dobeneck, T., Bickert, T., Dekkers, M. J., Frederichs, T., Meyer, I. and Zabel, M.: Multiproxy

596 characterization and budgeting of terrigenous end-members at the NW African continental margin, Geochem. Geophys.

597 Geosyst., 13(9), doi:10.1029/2012GC004148, 2012.

598 Koutavas, A. and Joanides, S.: El Niño-Southern Oscillation extrema in the Holocene and Last Glacial Maximum,

599 Paleoceanography, 27(4), doi:10.1029/2012pa002378, 2012.

21

600 Lagos, P., Silva, Y., Nickl, E. and Mosquera, K.: El Niño – related precipitation variability in Perú, Advances in Geosciences,
601 14, 231-237, doi:10.5194/adgeo-14-231-2008, 2008.

602 Mamalakis, A., Randerson, J., Yu, J., Pritchard, M., Magnusdottir, G., Smyth, P., Levine, P., Yu, S. and Foufoula-Georgiou,
603 E.: Zonally contrasting shifts of the tropical rain belt in response to climate change, Nature Climate Change, 11(2), 143-151,
604 doi:10.1038/s41558-020-00963-x, 2021.

605 Martin, L. C. P., Blard, P. H., Lavé, J., Condom, T., Prémaillon, M., Jomelli, V., Brunstein, D., Lupker, M., Charreau, J.,
606 Mariotti, V., Tibari, B., Team, A. and Davy, E.: Lake Tauca highstand (Heinrich Stadial 1a) driven by a southward shift of the
607 Bolivian High, Sci. Adv., 4(8), doi:10.1126/sciadv.aar2514, 2018.

608 McGee, D., Donohoe, A., Marshall, J. and Ferreira, D.: Changes in ITCZ location and cross-equatorial heat transport at the
609 Last Glacial Maximum, Heinrich Stadial 1, and the mid-Holocene, Earth Planet. Sci. Lett., 390, 69–79,
610 doi:10.1016/j.epsl.2013.12.043, 2014.

611 McManus, J. F., Francois, R., Gherardl, J. M., Kelgwin, L. and Drown-Leger, S.: Collapse and rapid resumption of Atlantic
612 meridional circulation linked to deglacial climate changes, Nature, 428(6985), 834–837, doi:10.1038/nature02494, 2004.

613 Mollier-Vogel, E., Leduc, G., Böschen, T., Martinez, P. and Schneider, R. R.: Rainfall response to orbital and millennial
614 forcing in northern Peru over the last 18ka, Quat. Sci. Rev., 76, 29–38, doi:10.1016/j.quascirev.2013.06.021, 2013.

615 Montade, V., Kageyama, M., Combourieu-Nebout, N., Ledru, M. P., Michel, E., Siani, G. and Kissel, C.: Teleconnection
616 between the intertropical convergence zone and southern westerly winds throughout the last deglaciation, Geology, 43(8),
617 735–738, doi:10.1130/G36745.1, 2015.

618 Morera, S., Condom, T., Crave, A., Steer, P. and Guyot, J.: The impact of extreme El Niño events on modern sediment transport
619 along the western Peruvian Andes (1968–2012), Scientific Reports, 7(1), doi:10.1038/s41598-017-12220-x, 2017.

620 Mulitza, S., Chiessi, C. M., Schefuß, E., Lippold, J., Wichmann, D., Antz, B., Mackensen, A., Paul, A., Prange, M., Rehfeld,
621 K., Werner, M., Bickert, T., Frank, N., Kuhnert, H., Lynch-Stieglitz, J., Portilho-Ramos, R. C., Sawakuchi, A. O., Schulz, M.,
622 Schwenk, T., Tiedemann, R., Vahlenkamp, M. and Zhang, Y.: Synchronous and proportional deglacial changes in Atlantic
623 meridional overturning and northeast Brazilian precipitation, Paleoceanography, 32(6), 622–633, doi:10.1002/2017PA003084,
624 2017.

625 Ng, H. C., Robinson, L. F., McManus, J. F., Mohamed, K. J., Jacobel, A. W., Ivanovic, R. F., Gregoire, L. J. and Chen, T.:
626 Coherent deglacial changes in western Atlantic Ocean circulation, Nat Commun, 9(1), doi:10.1038/s41467-018-05312-3,
627 2018.

628 Novello, V. F., Cruz, F. W., Vuille, M., Stríkis, N. M., Edwards, R. L., Cheng, H., Emerick, S., de Paula, M. S., Li, X., Barreto,
629 E. de S., Karmann, I. and Santos, R. V.: A high-resolution history of the South American Monsoon from Last Glacial Maximum
630 to the Holocene, Sci. Rep., 7(March), 44267, doi:10.1038/srep44267, 2017.

631 Ortlieb, L., Vargas, G. and Sali??ge, J. F.: Marine radiocarbon reservoir effect along the northern Chile-southern Peru coast
632 (14-24??S) throughout the Holocene, Quat. Res., 75(1), 91–103, doi:10.1016/j.yqres.2010.07.018, 2011.

633 Paterson, G. A. and Heslop, D.: New methods for unmixing sediment grain size data, Geochem. Geophys. Geosyst., 16(12),
634 4494–4506, doi:10.1002/2015GC006070, 2015.

635 Peterson, L., Haug, G., Hughen, K. and Röhl, U.: Rapid Changes in the Hydrologic Cycle of the Tropical Atlantic During the
636 Last Glacial, Science, 290(5498), 1947-1951, doi:10.1126/science.290.5498.1947, 2000.

637 Pettijohn, F.: Persistence of Heavy Minerals and Geologic Age, The Journal of Geology, 49(6), 610-625, doi:10.1086/624992,
638 1941.

639 Pichevin, L., Cremer, M., Giraudeau, J. and Bertrand, P.: A 190 ky record of lithogenic grain-size on the Namibian slope:
640 Forging a tight link between past wind-strength and coastal upwelling dynamics, Mar. Geol., 218(1–4), 81–96,
641 doi:10.1016/j.margeo.2005.04.003, 2005.

642 Rahmstorf, S., Box, J., Feulner, G., Mann, M., Robinson, A., Rutherford, S. and Schaffernicht, E.: Exceptional twentieth-
643 century slowdown in Atlantic Ocean overturning circulation, Nature Climate Change, 5(5), 475-480,
644 doi:10.1038/nclimate2554, 2015.

645 Rahn, D. and Garreaud, R.: A synoptic climatology of the near-surface wind along the west coast of South America,
646 International Journal of Climatology, 34(3), 780-792, doi:10.1002/joc.3724, 2013.

647 Rau, P., Bourrel, L., Labat, D., Melo, P., Dewitte, B., Frappart, F., Lavado, W. and Felipe, O.: Regionalization of rainfall over
648 the Peruvian Pacific slope and coast, International Journal of Climatology, 37(1), 143-158, doi:10.1002/joc.4693, 2016.

649 Rein, B., Lückge, A. and Sirocko, F.: A major Holocene ENSO anomaly during the Medieval period, Geophysical Research
650 Letters, 31(17), doi:10.1029/2004gl020161, 2004.

651 Rein, B., Lückge, A., Reinhardt, L., Sirocko, F., Wolf, A. and Dullo, W. C.: El Niño variability off Peru during the last 20,000
652 years, Paleoceanography, 20(4), 1–18, doi:10.1029/2004PA001099, 2005.

653 Reinhardt, L., Kudrass, H. R., Lückge, A., Wiedicke, M., Wunderlich, J., & Wendt, G.: High-resolution sediment
654 echosounding off Peru: Late Quaternary depositional sequences and sedimentary structures of a current-dominated
655 shelf, *Marine Geophysical Researches*, *23*(4), 335-35,2002

656 Salvatteci, R., Gutiérrez, D., Field, D., Sifeddine, A., Ortlieb, L., Bouloubassi, I., Boussafir, M., Boucher, H. and Cetin, F.:
657 The response of the Peruvian Upwelling Ecosystem to centennial-scale global change during the last two millennia, Clim.
658 Past, 10(2), 715–731, doi:10.5194/cp-10-715-2014, 2014a.

659 Salvatteci, R., Field, D., Sifeddine, A., Ortlieb, L., Ferreira, V., Baumgartner, T., Caquineau, S., Velazco, F., Reyss, J.,
660 Sanchez-Cabeza, J. and Gutierrez, D.: Cross-stratigraphies from a seismically active mud lens off Peru indicate horizontal
661 extensions of laminae, missing sequences, and a need for multiple cores for high resolution records, Marine Geology, 357, 72-
662 89, doi:10.1016/j.margeo.2014.07.008, 2014b.

663 Salvatteci, R., Gutierrez, D., Sifeddine, A., Ortlieb, L., Druffel, E., Boussafir, M. and Schneider, R.: Centennial to millennial-
664 scale changes in oxygenation and productivity in the Eastern Tropical South Pacific during the last 25,000 years, Quat. Sci.
665 Rev., 131, 102–117, doi:10.1016/j.quascirev.2015.10.044, 2016.

666 Salvatteci, R., Schneider, R. R., Blanz, T. and Mollier-Vogel, E.: Deglacial to Holocene Ocean Temperatures in the Humboldt
667 Current System as Indicated by Alkenone Paleothermometry, Geophys. Res. Lett., 46(1), 281–292,
668 doi:10.1029/2018GL080634, 2019.

669 Saukel, C., Lamy, F., Stuut, J. B. W., Tiedemann, R. and Vogt, C.: Distribution and provenance of wind-blown SE Pacific
670 surface sediments, Mar. Geol., 280(1–4), 130–142, doi:10.1016/j.margeo.2010.12.006, 2011.

671 Scheidegger, K. F. and Krissek, L. A.: Dispersal and deposition of eolian and fluvial sediments off Peru and northern Chile.,
672 Geol. Soc. Am. Bull., 93(2), 150–162, doi:10.1130/0016-7606(1982)93<150:DADOEA>2.0.CO;2, 1982.

673 Shakun, J. D., Clark, P. U., He, F., Marcott, S. A., Mix, A. C., Liu, Z., Otto-Bliesner, B., Schmittner, A. and Bard, E.: Global
674 warming preceded by increasing carbon dioxide concentrations during the last deglaciation, Nature, 484(7392), 49–54,
675 doi:10.1038/nature10915, 2012.

676 Sifeddine, A., Gutierrez, D., Ortlieb, L., Boucher, H., Velazco, F., Field, D., Vargas, G., Boussafir, M., Salvatteci, R., Ferreira,
677 V., García, M., Valdés, J., Caquineau, S., Mandeng Yogo, M., Cetin, F., Solis, J., Soler, P. and Baumgartner, T.: Laminated
678 sediments from the central Peruvian continental slope: A 500 year record of upwelling system productivity, terrestrial runoff
679 and redox conditions, Prog. Oceanogr., 79(2–4), 190–197, doi:10.1016/j.pocean.2008.10.024, 2008.

680 Stríkis, N. M., Chiessi, C. M., Cruz, F. W., Vuille, M., Cheng, H., De Souza Barreto, E. A., Mollenhauer, G., Kasten, S.,
681 Karmann, I., Edwards, R. L., Bernal, J. P. and Sales, H. D. R.: Timing and structure of Mega-SACZ events during Heinrich
682 Stadial 1, Geophys. Res. Lett., 42(13), 5477–5484, doi:10.1002/2015GL064048, 2015.

683 Stríkis, N., Cruz, F., Barreto, E., Naughton, F., Vuille, M., Cheng, H., Voelker, A., Zhang, H., Karmann, I., Edwards, R., Auler,
684 A., Santos, R. and Sales, H.: South American monsoon response to iceberg discharge in the North Atlantic, Proceedings of the
685 National Academy of Sciences, 115(15), 3788-3793, doi:10.1073/pnas.1717784115, 2018.

686 Strub, P. T., Mesias, J. M., Montecino, V., Rutllant, J., and Salinas, S.: Coastal ocean circulation off western South America,
687 in: The Sea, Vol. 11, edited by: Robinson, A. and Brink, K., John Wi- ley & Sons, New York, USA, 273–313, 1998.

688 Stuut, J. B. W., Kasten, S., Lamy, F. and Hebbeln, D.: Sources and modes of terrigenous sediment input to the Chilean
689 continental slope, Quat. Int., 161(1), 67–76, doi:10.1016/j.quaint.2006.10.041, 2007.

690 Stuut, J. B. W., Prins, M. A., Schneider, R. R., Weltje, G. J., Fred Jansen, J. H. and Postma, G.: A 300-kyr record of aridity
691 and wind strength in southwestern Africa: Inferences from grain-size distributions of sediments on Walvis Ridge, SE Atlantic,
692 Mar. Geol., 180(1–4), 221–233, doi:10.1016/S0025-3227(01)00215-8, 2002.

693 Stuut, J. B. W., Temmesfeld, F. and De Deckker, P.: A 550ka record of aeolian activity near north west cape, australia:
694 Inferences from grain-size distributions and bulk chemistry of SE indian ocean deep-sea sediments, Quat. Sci. Rev., 83, 83–
695 94, doi:10.1016/j.quascirev.2013.11.003, 2014.

696 Stuut, J.-B. W. and Lamy, F.: Climate variability at the southern boundaries of the Namib (southwestern Africa) and Atacama
697 (northern Chile) coastal deserts during the last 120,000 yr, Quat. res., 62(3), 301–309, doi:10.1016/j.yqres.2004.08.001, 2004.

698 Suess, E., Kulm, L. D. and Killingley, J. S.: Coastal upwelling and a history of organic-rich mudstone deposition off Peru,
699 Geological Society, London, Special Publications, 26(1), 181–197, doi:10.1144/GSL.SP.1987.026.01.11, 1987.

24

700 Sublette Mosblech, N., Chepstow-Lusty, A., Valencia, B. and Bush, M.: Anthropogenic control of late-Holocene landscapes
701 in the Cuzco region, Peru, The Holocene, 22(12), 1361-1372, doi:10.1177/0959683612449760, 2012.

702 Vuille, M., Burns, S., Taylor, B., Cruz, F., Bird, B., Abbott, M., Kanner, L., Cheng, H. and Novello, V.: A review of the South
703 American monsoon history as recorded in stable isotopic proxies over the past two millennia, Climate of the Past, 8(4), 1309-
704 1321, doi:10.5194/cp-8-1309-2012, 2012.

705 Weltje, G. J. and Prins, M. A.: Genetically meaningful decomposition of grain-size distributions, Sedimentary Geology,
706 202(3), 409–424, doi:10.1016/j.sedgeo.2007.03.007, 2007.

707 Weltje, G. J. and Prins, M. A.: Muddled or mixed? Inferring palaeoclimate from size distributions of deep-sea clastics,
708 Sedimentary Geology, 162(1–2), 39–62, doi:10.1016/s0037-0738(03)00235-5, 2003.

709 Wu, L., Wilson, D., Wang, R., Yin, X., Chen, Z., Xiao, W. and Huang, M.: Evaluating Zr/Rb Ratio From XRF Scanning as an
710 Indicator of Grain-Size Variations of Glaciomarine Sediments in the Southern Ocean, Geochemistry, Geophysics, Geosystems,
711 21(11), doi:10.1029/2020gc009350, 2020.

712 Yarincik, K., Murray, R. and Peterson, L.: Climatically sensitive eolian and hemipelagic deposition in the Cariaco Basin,
713 Venezuela, over the past 578,000 years: Results from Al/Ti and K/Al, Paleoceanography, 15(2), 210-228,
714 doi:10.1029/1999pa900048, 2000.

715 Zhang, Y., Chiessi, C. M., Mulitza, S., Zabel, M., Trindade, R. I. F., Helena, M., Hollanda, B. M., Dantas, E. L., Govin, A.,
716 Tiedemann, R. and Wefer, G.: Origin of increased terrigenous supply to the NE South American continental margin during
717 Heinrich Stadial 1 and the Younger Dryas, Earth Planet. Sci. Lett., 432, 493–500, doi:10.1016/j.epsl.2015.09.054, 2015.

718 Zhou, W., Leung, L., Lu, J., Yang, D. and Song, F.: Contrasting Recent and Future ITCZ Changes From Distinct Tropical
719 Warming Patterns, Geophysical Research Letters, 47(22), doi:10.1029/2020gl089846, 2020.

720